IOP Publishing Physica Scripta
Phys. Scr. 95 (2020) 055006 (10pp) https://doi.org/10.1088/1402-4896/ab6da2

Numerical treatment of slip velocity and catheterization on the gravity flow of non-Newtonian fluid model through a uniform blood vessel

Z Abbas[1], B Iftikhar[1], M S Shabbir[1,4], M Alghamdi[2] and J Iqbal[3]

[1] Department of Mathematics, The Islamia University of Bahawalpur, Bahawalpur 63100, Pakistan
[2] Department of Mathematics, Faculty of Science, King Khalid University, Abha 61413, Saudi Arabia
[3] Government College of Technology for Women, Bahawalpur 63100, Pakistan

E-mail: shahzad.6@hotmail.com

Received 9 October 2019, revised 31 December 2019
Accepted for publication 20 January 2020
Published 13 March 2020

Abstract

The aim of the present article is to investigate the influence of gravity and slip velocity on the steady flow of blood through an inclined catheterized blood vessel. The constitutive relation of Herschel–Bulkley fluid is utilized to capture the non-Newtonian characteristics of the blood. The effects of catheter radius, yield stress, slip velocity and the inclination angle on the velocity, flow rate, wall shear stress and resistance to the flow are analyzed in detail. The expression of velocity is evaluated numerically by using Regula falsi method. The variation of different flow variables corresponding to the involved geometric and rheologic parameters is shown through graphs. It is shown that the velocity decreases as the yield stress attains higher values. The yield stress enhances the impedance and wall shear stress. Increase in the catheter radius reduces the wall shear stress and resistive impedance. The study also reveals that the impedance for horizontal blood vessel is higher as compared to the vertical blood vessel.

Keywords: catheterized inclined artery, slip condition, yield planes, Herschel–Bulkley fluid, resistance to flow

1. Introduction

In the current times with the advancement of coronary balloon angioplasty, the utilization of catheters of several sizes has been considerably increased. Catheterization is a procedure used to insert a long thin elastic tube in the blood vessels. Angiography is the type of heart catheter procedure for the diagnosis of heart related diseases. The presence of the catheter in the artery forms an annular region between the arterial wall and the catheter wall. As the small catheter is inserted in an artery, the frictional resistance is increased within the artery. Hence the flow field is altered and pressure distribution is modified. The purpose of catheters includes accurately measurement of pressure gradient, and clearing of occlusions from the walls of the diseased artery [1]. Back [2] measured the resistance to the flow in case of Newtonian flow of blood. He reported that even a very small size of angioplasty guide-wire leads to sizable increase in flow resistance. The pressure or pressure gradient recorded by a transducer attached to the catheter will differ from that of an uncatheterized artery and it is essential to know the catheter induced error. Recently, the relationship between flow patterns and atheroma formation has been studied by using coronary catheter probes in conjunction with computational fluid dynamics [3].

The estimates of wall shear stress were studied by Back and Denton [4] and its scientific importance is discussed in coronary angioplasty. In routine animal experiments and scientific studies, the arterial flow velocityflow rate and blood pressure/pressure gradient measurements in the required part of the arterial network is generally achieved using a suitable catheter-tool device (such as a catheter tip flow meter or catheter transducer system). Catheters are also utilized in diagnostic procedures (e.g.

[4] Author to whom any correspondence should be addressed.

intravascular ultrasound, X-ray angiography) as well as in the healing techniques (e.g. balloon angioplasty) of several arterial diseases. Back [1] and Back *et al* [5] investigated the main hemodynamic features like the pressure drop, resistance and wall shear stress in coronary catheterized arteries under typical as well as the clinical state of a stenosis present. Blood has been considered as a Newtonian fluid in all the above studies. But it is renowned that, being deferment of cells, blood acts as a non-Newtonian fluid through its flow in narrow blood vessels and at low shear rates. In small blood vessels, the pulsatile flow of blood was studied by Aroesty and Gross [6] and their theory was extended by Chaturani and Ponnalagar Samy [7] to investigate pulsatile blood flow by modeling blood as a Casson fluid in stenosed arteries.

The catheterization effects on several flow properties in an artery which is curved was investigated by Tiwari and Jayaraman [8] and Karahalios [9] considering blood as a Newtonian fluid. When a catheter is injected into a narrow artery, the changed flow pattern was investigated by Dash *et al* [10] and the frictional growth in the artery caused by catheterization was estimated by using the Casson model for blood. Dash *et al* [11] used toroidal coordinate system to study the steady Newtonian flow of blood in stenotic catheterized curved artery. Daripa *et al* [12] have studied numerically using a fast algorithm the pulsatile blood flow in an eccentric catheterized artery considering blood alike a type of Newtonian fluid. Vajravelu *et al* [13] have investigated the peristaltic transport of blood in an inclined tube by blood of modeling as Herschel–Bulkley fluid. Sankar and Hemalatha [14] used perturbation method to study the pulsatile flow of Herschel–Bulkley across the arteries with catheterized.

Spanner *et al* [15] stated that the blood follows Casson fluid equation only in the bounded range, but at very low and very high shear rate and that there is no division between the Herschel– Bulkley plots and Casson plots over the range of experimental data where the Casson plot is valid. It is noted that the model of Casson fluid can be applied for usual shear rates $C < 10/\mathrm{s}$ in tubes of smaller diameter. However, the model of Herschel–Bulkley, fluid can be applied in very narrow arteries at yet a lower shear rate of flow where the θ as yield stress is high [15, 16]. As the Herschel–Bulkley equation includes one more parameter than the Casson equation, it would be estimated that the use of the Herschel–Bulkley equation gives more detailed evidence about blood properties. Moreover, the Herschel–Bulkley fluid equation can be used to explain the behavior of power law fluid, Newtonian and Bingham fluid by reading suitable values of the parameters.

It has been indicated by both Scott Blair [17] and Iida [18] that model of Herschel–Bulkley is more suitable and farther common for a blood flow although it is likely to model the same flow by both Herschel–Bulkley fluid and Casson fluid concluded the range in which both models are acceptable. Scott Blair [17] has indicated that the sum of the squares of the differences between the examined and estimated the shear stress values was lowest for Herschel–Bulkley than Casson fluid model, but the investigation is more complicated for fluid of Herschel–Bulkley. Iida [18] testified that the velocity is usually explained by the two models accurately in the arterioles taking a diameter less than 100 μm. Zaman *et al* [19] examined the unsteady blood flow in a catheterized stenotic artery including post stenotic dilatation in a micropolar hemodynamics model.

Recently, Abbas *et al* [20, 21] comparatively studied the flow of blood by using the Herschel–Bulkley fluid model through the arteries having single symmetric, overlapping and multi-triangular stenosis. They pointed out that the shape of the stenosis has significant effect on the flow variables. Chitra and Karthikeyan [22] explored the effects of slip velocity and permeability wall of the artery by considering the Herschel–Bulkley fluid model. Maruthi Prasad, and Radhakrishnamacharya [23] analyzed the influence of various parameter on the shear stress and resistance to the flow for Herschel–Bulkley fluid in an inclined artery having non-uniform cross section. Some useful studies regarding the flow of different non-Newtonian fluid models are referenced in the literature [24–30]. Motivated by the above discussion an attempt has been made to highlight the effects of slip velocity on the different flow variables in case of steady flow of blood through a catheterized artery. The Herschel–Bulkley fluid model is utilized for the representation of rheological behavior of the blood. We have make use of the technique introduced by Sankar and Hemalatha [30] and extend their findings by incorporating the effects of inclined blood vessel and the slip boundary condition.

The present article is organized as: section 2 deals with the formulation of the problem with appropriate assumptions. In section 3, the flow problem is non-dimensionalized and is solved by using numerical techniques. Section 4 comprises with the effects of catheterization on velocity, wall shear stress, the rate of flow and impedance for distinct values of the parameters for Herschel–Bulkley fluid mode and the results for power law and Bingham fluid are discussed as the special case of Herschel–Bulkley fluid.

2. Formulation of the problem

Consider the flow of blood in an inclined artery in which a coaxially catheter is inserted. The artery is shaped as a circular rigid tube having radius $\bar{R}$. The blood is modeled by Herschel–Bulkley fluid the radius of catheter is chosen to be $k\bar{R}$ $(k < 1)$. The flow is supposed to be steady, laminar, axially symmetric and fully developed. There is a slip condition acting on the wall of the artery. The cylindrical polar coordinates (r, ϕ, z), where z and r are the axial and radial coordinates and ϕ is termed as the azimuthal angle, shown in figure 1.

It is also indicated that the magnitude of radial velocity is negligibly small and can be neglected for low Reynolds number flow and the pressure gradient is a function of z alone. In this case, the momentum equation shortens to

$$\frac{\partial \bar{p}}{\partial \bar{z}} = -\frac{1}{\bar{r}}\frac{\mathrm{d}}{\mathrm{d}\,\bar{r}}(\bar{\tau}\,\bar{r}) + \bar{\rho} g \sin\psi,\ k\bar{R} \leqslant \bar{r} \leqslant \bar{R}, \qquad (1)$$

where $\bar{\tau}$ denotes the shear stress, $\bar{p}$ symbolizes the pressure, $\bar{\rho}$ symbolizes the density, g denotes the gravitational force and

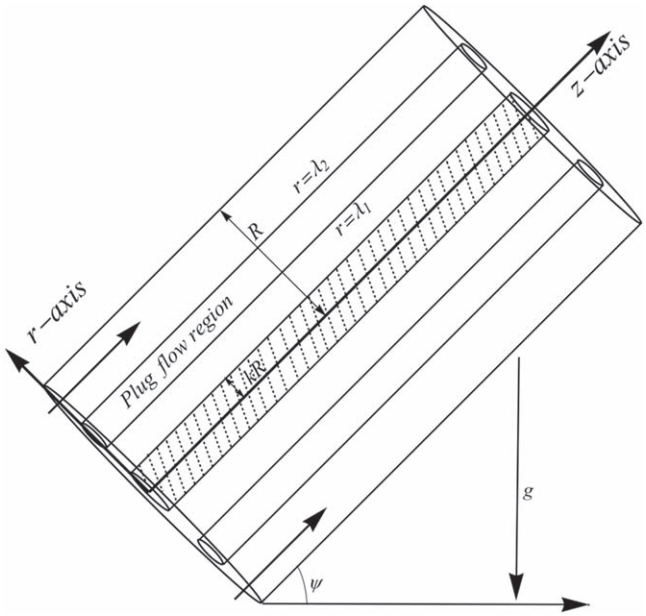

Figure 1. Geometry of catheterized inclined artery.

ψ is the inclination angle of the artery. The constitutive equation for Herschel–Bulkley fluid in general form is given as [14]

$$\bar{\eta}\left|\frac{\partial \bar{u}}{\partial \bar{r}}\right| = (|\bar{\tau}| - \bar{\tau}_y)^n, \text{ for } |\bar{\tau}| \geqslant \bar{\tau}_y, \tag{2}$$

$$\frac{\partial \bar{u}}{\partial \bar{r}} = 0, \text{ for } |\bar{\tau}| \geqslant \bar{\tau}_y, \tag{3}$$

where $\bar{\tau}_y$ is the known as yield stress, $\bar{u}$ is called the axial velocity, n is termed as the power index and $\bar{\eta}$ is the well-known viscosity coefficient having dimension $(ML^{-1}T^{-2})^nT$, for Herschel–Bulkley fluid. When strain rate and shear stress have signs opposite to each other and when $|\bar{\tau}| \geqslant \bar{\tau}_y$, the corresponding form of these relations can be written as

$$\bar{\eta}\frac{\partial \bar{u}}{\partial \bar{r}} = (|\bar{\tau}| - \bar{\tau}_y)^n, \text{ for } \frac{\partial \bar{u}}{\partial \bar{r}} > 0 \text{ and } \bar{\tau} < 0 \tag{4}$$

$$= -(|\bar{\tau}| - \bar{\tau}_y)^n, \text{ for } \frac{\partial \bar{u}}{\partial \bar{r}} < 0 \text{ and } \bar{\tau} > 0. \tag{5}$$

For $\frac{\bar{\tau}_y}{|\bar{\tau}|} \ll 1$, the higher powers of $\frac{\bar{\tau}_y}{|\bar{\tau}|}$ can be neglected and above constitutive equation can be written as

$$\bar{\eta}\frac{\partial \bar{u}}{\partial \bar{r}} = |\bar{\tau}|^n\left(1 - \frac{n\bar{\tau}_y}{|\bar{\tau}|}\right), \text{ if } |\bar{\tau}| \geqslant \bar{\tau}_y \text{ and } \frac{\partial \bar{u}}{\partial \bar{r}} > 0, \tag{6}$$

$$\bar{\eta}\frac{\partial \bar{u}}{\partial \bar{r}} = -|\bar{\tau}|^n\left(1 - \frac{n\bar{\tau}_y}{|\bar{\tau}|}\right), \text{ if } |\bar{\tau}| \geqslant \bar{\tau}_y \text{ and } \frac{\partial\, \bar{u}}{\partial\, \bar{r}} < 0 \tag{7}$$

$$= 0 \text{ if } |\bar{\tau}| < \bar{\tau}_y. \tag{8}$$

When slip boundary condition on the wall of the artery is applied, equations (1) and (6)–(8) can be solved as given by

$$\bar{u}(\bar{r} = k\bar{R}) = 0, \tag{9}$$

$$\bar{u}(\bar{r} = \bar{R}) = a_s, \tag{10}$$

where a_s is the slip velocity.

3. Solution of the problem

Let $\bar{\eta}$ is the coefficient of viscosity for Herschel–Bulkley fluid given as

$$\bar{\eta} = \bar{\mu}^n\left(\frac{\bar{u}}{\bar{R}}\right)^{n-1}. \tag{11}$$

The following non-dimensional variables are used:

$$u = \frac{\bar{u}}{u_0}, \tau = \frac{\bar{\tau}}{\mu\left(\frac{u_0}{R}\right)}, r = \frac{\bar{r}}{\bar{R}}, z = \frac{\bar{z}}{\bar{R}},$$

$$Re = \frac{\bar{\rho}\, u_0\bar{R}}{\mu}, \; Fr = \frac{{u_0}^2}{g\,\bar{R}}. \tag{12}$$

The pressure gradient in this case can be written as:

$$-\frac{\mathrm{d}p}{\mathrm{d}z} = p_s. \tag{13}$$

Non-dimensional form of the momentum equation (1) is given by

$$-p_s + \frac{1}{r}\frac{\mathrm{d}}{\mathrm{d}r}(r\tau) = \frac{R_e}{f_r}\sin\psi, \; k \leqslant r \leqslant 1. \tag{14}$$

The non-dimensional form of the constitutive equations (6)–(8) is

$$\frac{\partial u}{\partial r} = |\tau|^n\left(1 - \frac{n\theta}{|\tau|}\right), \text{ if } |\tau| \geqslant \theta \text{ and } \frac{\partial u}{\partial r} > 0 \tag{15}$$

$$\frac{\partial u}{\partial r} = -|\tau|^n\left(1 - \frac{n\theta}{|\tau|}\right), \text{ if } |\tau| \geqslant \theta \text{ and } \frac{\partial u}{\partial r} < 0 \tag{16}$$

$$= 0, \text{ if } |\tau| < \theta, \tag{17}$$

where

$$\theta = \frac{\bar{R}\bar{\tau}_y}{\bar{\mu}u_0} \tag{18}$$

is the yield stress in non-dimensional form. The boundary conditions (9), (10) reduce to

$$u(r = k) = 0, \tag{19}$$

$$u(r = 1) = U_0. \tag{20}$$

Integration of equation (14) gives

$$\tau = \frac{p_s r}{2} + \frac{R_e}{f_r}\frac{r}{2}\sin\psi + \frac{c}{r}, \tag{21}$$

where c is called constant of integration. From equations (15)–(17), it is obvious that the flow is in three regions (as in figure 1) one for $k \leqslant r \leqslant 1$, in which the main core has smooth velocity profile and thus creates the plug flow area. The shear stress in the plug flow area does not exceed the yield stress and the fluid streamlines are moving with same velocities, so the flow is not sheared. For mathematical demonstration, suppose this plug flow area be define by $\lambda_1 \leqslant r \leqslant \lambda_2$, where $k \leqslant \lambda_1$, $\lambda_2 \leqslant 1$, λ_1 and λ_2 are indefinite quantities to be calculated. From the continuous shear stress alongside the boundary of the plug core flow area, we have

$$-\tau|_{r=\lambda_1} = \theta = \tau|_{r=\lambda_2}. \tag{22}$$

Using the above equation (22) in (13), we get

$$c = p_s(\lambda^2) + \frac{R_e}{f_r}\frac{1}{2}\sin\psi(\lambda^2), \tag{23}$$

where

$$\lambda^2 = (\lambda_1\lambda_2). \tag{24}$$

Substitution of equation (23) in (21) yield the shear stress is

$$\tau = \frac{p_s}{r}(r^2 - \lambda^2) + \frac{R_e}{f_r}\frac{1}{2}\sin\psi(r^2 - \lambda^2). \tag{25}$$

Using equations (25) and (22) we have

$$(\lambda_2 - \lambda_1) = \frac{\theta}{p_s} = \alpha_s \text{ (say)}, \tag{26}$$

where α_s is the plug core area's width. In three regions, the terms for the velocity can be attained from equations (25) and (15)–(17) and the boundary condition (19), (20) given by

$$\begin{aligned} u^+(r) = {} & p_s^n\int_k^r\left(\left(\frac{\lambda^2 - r^2}{r}\right) + \frac{R_e}{f_r}\frac{1}{2}\sin\psi\right. \\ & \left.\times\left(\frac{\lambda^2 - r^2}{r}\right)\right)^n \mathrm{d}r \\ & - n\alpha_s\left[\int_k^r\left(\left(\frac{\lambda^2 - r^2}{r}\right) + \frac{R_e}{f_r}\frac{1}{2}\sin\psi\right.\right. \\ & \left.\left.\times\left(\frac{\lambda^2 - r^2}{r}\right)\right)^{n-1}\mathrm{d}r\right] \text{when } k \leqslant r \leqslant \lambda_1 \end{aligned} \tag{27}$$

$$u_p(r) = \text{constant, when } \lambda_1 \leqslant r \leqslant \lambda_2 \tag{28}$$

$$\begin{aligned} u^{++}(r) = {} & U_0 + p_s^n\int_r^1\left(\left(\frac{r^2 - \lambda^2}{r}\right) + \frac{R_e}{f_r}\frac{1}{2}\sin\psi\right. \\ & \left.\times\left(\frac{r^2 - \lambda^2}{r}\right)\right)^n \mathrm{d}r \\ & - n\alpha_s\left[\int_r^1\left(\left(\frac{r^2 - \lambda^2}{r}\right) + \frac{R_e}{f_r}\frac{1}{2}\sin\psi\right.\right. \\ & \left.\left.\times\left(\frac{r^2 - \lambda^2}{r}\right)\right)^{n-1}\mathrm{d}r\right] \text{when } \lambda_2 \leqslant r \leqslant 1, \end{aligned} \tag{29}$$

where plug flow velocity is denoted by u_p. As $\alpha_s = 0$, when there is no yield stress ($\theta = 0$), equations (27) and (29) give the velocity profile for a fluid of power law in a catheterized tube. This corresponds with the result noted by Kapur [31]. When the inclination angle $\psi = 0$ $\psi = 0$, the resultant equations (27) and (29) corresponds to the results studied by Sankar [30]. Throughout the flow field, continuity of the distribution of velocity precedes to the condition

$$u^+(r = \lambda_1) = u_p = u^{++}(r = \lambda_2) \tag{30}$$

which leads to

$$\begin{aligned} & p_s^n\int_k^{\lambda_1}\left(\left(\frac{\lambda^2 - r^2}{r}\right) + \frac{R_e}{f_r}\frac{1}{2}\sin\psi\left(\frac{\lambda^2 - r^2}{r}\right)\right)^n \mathrm{d}r \\ & - p_s^n\int_{\lambda_2}^1\left(\left(\frac{r^2 - \lambda^2}{r}\right) + \frac{R_e}{f_r}\frac{1}{2}\sin\psi\left(\frac{r^2 - \lambda^2}{r}\right)\right)^n \mathrm{d}r \\ & -n\alpha_s\left[\int_k^{\lambda_1}\left(\left(\frac{\lambda^2 - r^2}{r}\right) + \frac{R_e}{f_r}\frac{1}{2}\sin\psi\left(\frac{\lambda^2 - r^2}{r}\right)\right)^{n-1}\mathrm{d}r\right. \\ & \left. -\int_{\lambda_2}^1\left(\left(\frac{r^2 - \lambda^2}{r}\right) + \frac{R_e}{f_r}\frac{1}{2}\sin\psi\left(\frac{r^2 - \lambda^2}{r}\right)\right)^{n-1}\mathrm{d}r\right] \\ & -U_0 = 0. \end{aligned} \tag{31}$$

Using $\lambda^2 = (\lambda_1\lambda_2)$ and equation (26), the equation (31) lessens to the integral form equation in λ_1 given by

$$\begin{aligned} & p_s^n\int_k^{\lambda_1}\left(\left(\frac{\lambda_1(\lambda_1 + \beta_s) - r^2}{r}\right) + \frac{R_e}{f_r}\frac{1}{2}\sin\psi\right. \\ & \left.\times\left(\frac{\lambda_1(\lambda_1 + \beta_s) - r^2}{r}\right)\right)^n \mathrm{d}r \\ & - p_s^n\int_{\lambda_2}^1\left(\left(\frac{r^2 - \lambda_1(\lambda_1 + \beta_s)}{r}\right) + \frac{R_e}{f_r}\frac{1}{2}\sin\psi\right. \\ & \left.\times\left(\frac{r^2 - \lambda_1(\lambda_1 + \beta_s)}{r}\right)\right)^n \mathrm{d}r \\ & -n\alpha_s\left[\int_k^{\lambda_1}\left(\left(\frac{\lambda_1(\lambda_1 + \beta_s) - r^2}{r}\right) + \frac{R_e}{f_r}\frac{1}{2}\sin\psi\right.\right. \\ & \left.\left.\times\left(\frac{\lambda_1(\lambda_1 + \beta_s) - r^2}{r}\right)\right)^{n-1}\mathrm{d}r\right. \\ & \left. -\int_{\lambda_2}^1\left(\left(\frac{r^2 - \lambda_1(\lambda_1 + \beta_s)}{r}\right) + \frac{R_e}{f_r}\frac{1}{2}\sin\psi\right.\right. \\ & \left.\left.\times\left(\frac{r^2 - \lambda_1(\lambda_1 + \beta_s)}{r}\right)\right)^{n-1}\mathrm{d}r\right] - U_0 = 0. \end{aligned} \tag{32}$$

The above equation (32) is numerically solved for λ_1 by applying Regula-Falsi method. Trapezoidal rule is used to evaluate the integrals in equation (32). When λ_1 is known, equation (26) is used to determine λ_2. The relations of velocity can be attained from equations (27)–(29) and applying equation (24). The steady flow rate Q_s is given by [30]

$$\begin{aligned} Q_s = 8\int_k^1 r\,u\,\mathrm{d}r = 4p_s^n\left[\int_k^{\lambda_1}\left\{n\beta_s\left(\frac{\lambda^2 - r^2}{r}\right)^{n-1}\right.\right. \\ \left. - \left(\frac{\lambda^2 - r^2}{r}\right)^n\right\}r^2\mathrm{d}r + \int_{\lambda_2}^1\left\{\left(\frac{r^2 - \lambda^2}{r}\right)^n\right. \\ \left.\left. - n\beta_s\left(\frac{r^2 - \lambda^2}{r}\right)^{n-1}\right\}r^2\mathrm{d}r\right]. \end{aligned} \tag{33}$$

In the artery, the wall shear stress is determined from equation (25) with $r = 1$ and given as

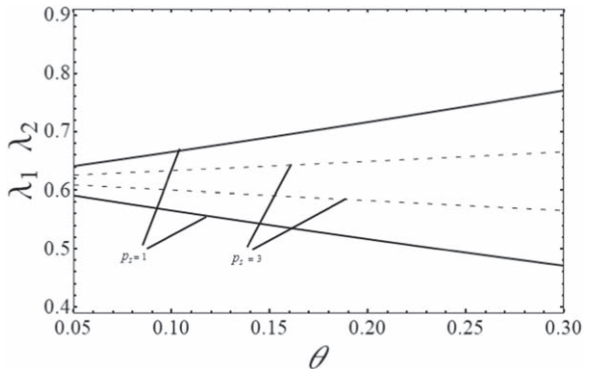

Figure 2. Variation of yield plane locations with θ as yield stress for distinct values of pressure gradient p_s while $k = 0.5$, $\theta = 0.1$, $n = 0.95$, $U_0 = 0.005$, $\psi = 45^\circ$ and $R_e/f_r = 0.2$.

$$\tau_w = p_s(1 - \lambda^2) + \frac{R_e}{f_r}\frac{1}{2}\sin\psi(1 - \lambda^2). \tag{34}$$

The τ_w as wall shear stress, for fixed value of p_s depends on λ which sequentially depends on θ and k. In the artery, the per unit length frictional resistance is given as [20]

$$\Lambda = \frac{p_s}{Q_s}. \tag{35}$$

4. Results and discussions

The purpose of the present analysis is to comprehend the blood flow through a catheterized inclined artery and to introduce the prominent aspects of the flow pattern and to evaluate the flow resistance due to the existence of a catheter in a small artery by assuming the constitutive equation of the flow is supposed to be steady. This model has a key advantage that it includes the Newtonian model and fluid of power law model as specific cases, so that in current analysis, blood flow modeling by fluids without yield stress through larger arteries can also be attained. Sankar [30] reported that the value of yield stress of blood for normal human being lies between 0.04 and 0.06 but it is higher in the diseased condition so we have taken the values of yield stress between 0 and 0.3. Also the values of catheter radius are chosen from 0.1 to 0.7 to accommodate all types of the catheters. The values of the power law index are chosen to be 0.95 (for $n < 1$) and 1.05 (for $n > 1$).

Figure 2 shows the λ_1 and λ_2 as yield plane position with θ as yield stress for distinct values of pressure gradient with $n = 0.95$, $\psi = 45^\circ$, $k = 0.3$, and the ratio of R_e and f_r is 0.2. for a certain value of r, k, ψ, and θ, the width is k of the plug core area decreases and the value of λ_1 increases with increases pressure gradient p_s.

Figure 3 is plotted to show the variation of axial velocity for distinct values of θ with $n = 0.95$. It is observed that the velocity decreases by increasing the yield stress parameter θ. It is also evident from the figure that the velocity in case of power law fluid model is higher than those for Newtonian and Herschel–Bulkley fluid. Figure 4 is depicted to show the

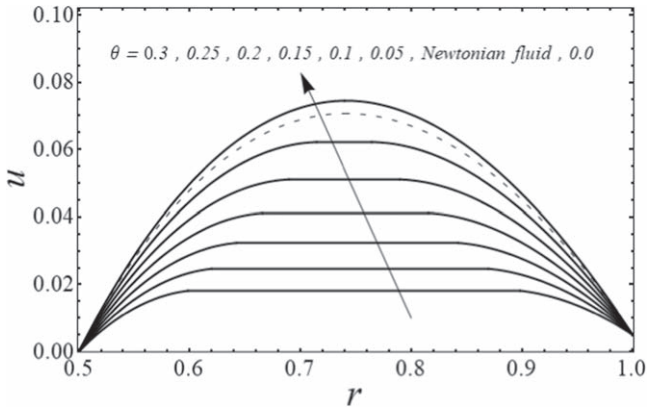

Figure 3. Velocity profile for distinct values of θ as yield stress with $k = 0.5$ and $p_s = 1$, $n = 0.95$, $\psi = 45^\circ$, $U_0 = 0.005$ and $R_e/f_r = 0.2$.

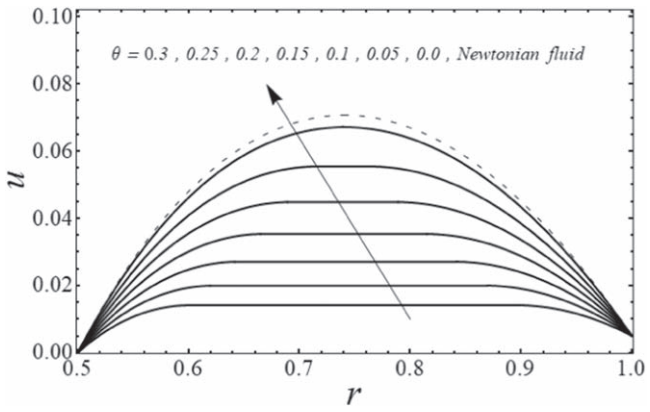

Figure 4. Velocity profile for distinct values of θ as yield stress with $p_s = 1$, $k = 0.5$, $U_0 = 0.005$, $\psi = 45^\circ$, $n = 1.05$ and $R_e/f_r = 0.2$

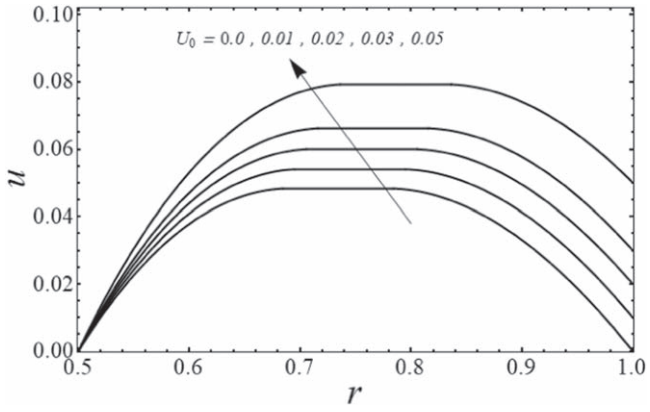

Figure 5. Velocity profile for distinct values of slip parameter U_0 with $k = 0.5$, $p_s = 1$, $\theta = 0.1$, $n = 0.95$, $\psi = 45^\circ$ and $R_e/f_r = 0.2$.

distribution of axial velocity for different values of θ with $n = 1.05$. It is remarkable to note that the Newtonian fluid velocity is higher in the present case while the velocities of power law fluid and Herschel–Bulkley fluid are comparatively smaller.

Figure 5 reveals the influence of the slip velocity on the radial distribution of the axial velocity. It is observed that the

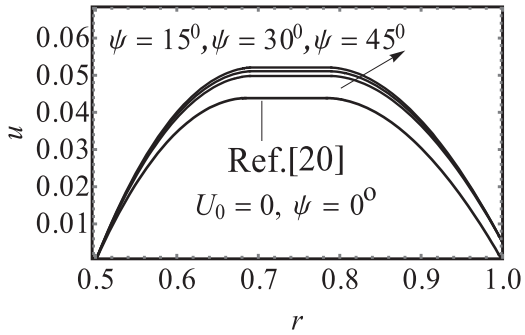

Figure 6. Velocity profile for distinct values inclination angle ψ with $= 0.5$, $p_s = 1$, $\theta = 0.1$, $n = 0.95$, $U_0 = 0.005$ and $R_e/f_r = 0.2$.

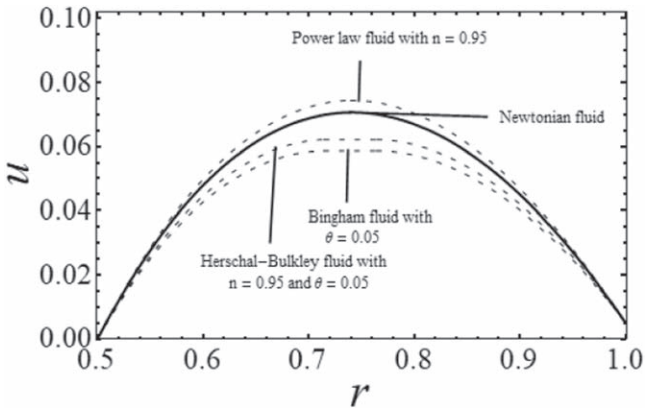

Figure 7. Velocity profile for several fluids with $p_s = 1$, $k = 0.5$, $U_0 = 0.005$, $\psi = 45^\circ$ and $R_e/f_r = 0.2$

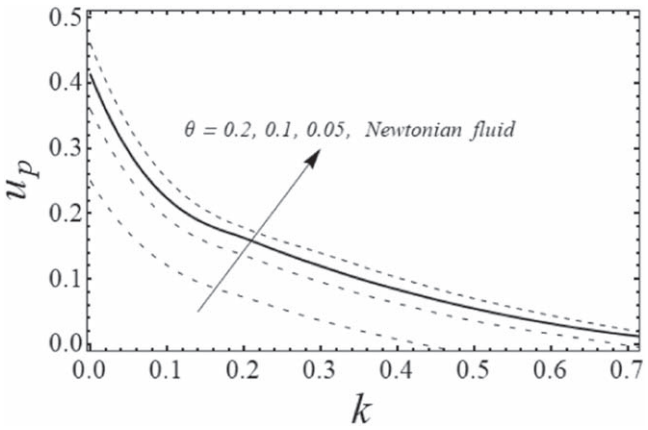

Figure 8. Change the flow of plug velocity with k as catheter radius ratio for distinct values of θ as yield stress with $p_s = 1$, $n = 0.95$, $\psi = 45^\circ$, $U_0 = 0.005$ and $R_e/f_r = 0.2$.

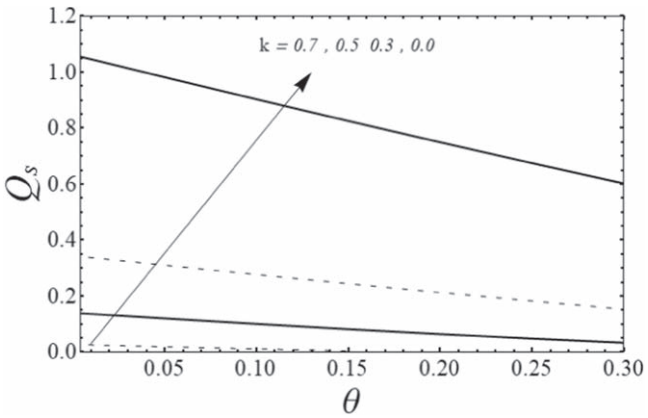

Figure 9. Change the rate of flow with θ as yield stress for distinct values of k as catheter radius ratio with $p_s = 1$, $n = 0.95$, $\psi = 45^\circ$, $U_0 = 0.005$ and $R_e/f_r = 0.2$.

magnitude of the axial velocity increases by increasing the slip velocity. The variation of the velocity with the inclination parameter ψ is shown in figure 6. Figure 6 also shows that our results are in good agreement with the results reported by Sankar [30]. Increase in the velocity is noted for the increasing value of ψ. Figure 7 is constructed to highlight the effects of slip velocity on different fluids. The figure shows that the velocity of power law is maximum while for Bingham fluid it is minimum. Figure 8 shows the plug core velocity variation with respect to catheter ratio k for distinct values of yield stress θ with $n = 0.95$ and $\psi = 45^\circ$. For each value of θ, when k increases from 0 to 0.15 the plug flow velocity reduces rapidly and when k varies from 0.15 to 0.7, the velocity reduces gradually. The plug flow velocity equals to zero for $\theta = 0.2$ and when k is approximately 0.45. The change in the flow rate with respect to yield stress parameter θ for distinct values of catheter radius ratio k and unit pressure gradient are indicated in figure 9. The rate of flow reduces approximately linearly with respect to θ. Figure 9 also illustrates the change of steady flow rate with respect to the yield stress θ for a several values of catheter radius ratio k. The figure shows that the flow rate reduces approximately linearly with respect to θ. Also any growth in the catheter radius k reduces the flow rate. This is due to the fact that the angular flow area decreases by increasing k.

Change in the steady flow rate with respect to pressure gradient p_s for distinct values of θ are shown in figure 10. It is observed that the θ has comparable effect on the variation of steady flow rate. The yield stress θ has positive influence on the steady flow rate. These effects are more prominent for higher value of p_s. Figure 11 highlights the influence of power law index n on the steady flow rate plotted with respect to different values of pressure gradient. The figure show that the flow rate decreases by increasing n are more comparable for higher value of p_s.

The variation of the flow rate verses pressure gradient for distinct values of U_0 is displayed in the figure 12. From the figure it is noted that the value of the flow rate increase by decreasing value of slip parameter U_0 for a specified pressure gradient p_s. The change in the flow rate verses, p_s for distinct values of ψ is displayed in the figure 13. It is noted that increase in the inclination angle results in the higher values of the flow rate for a specified p_s gradient of pressure. Figure 14 indicates the wall shear stress variations for distinct values of yield stress θ. For a specified pressure gradient p_s, it is seen that the catheter radius ratio k is increased as the walls shear stress is decreased. The wall shear stress increases slightly for

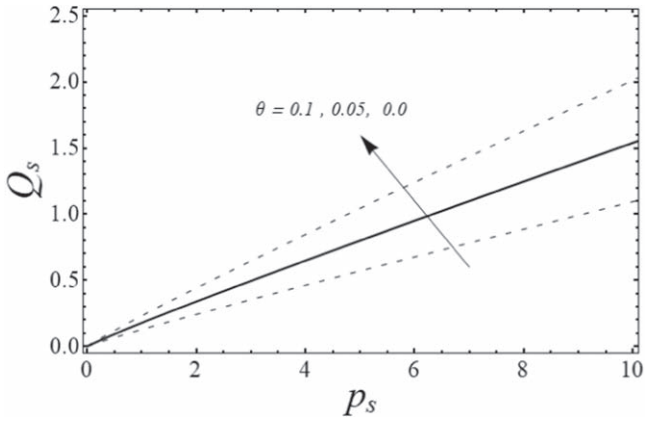

Figure 10. Change the rate of flow with p_s as pressure gradient for distinct values of yield stress θ with catheter radius ratio $k = 0.4$, $n = 0.95$, $\Psi = 45^{\circ}$, $U_0 = 0.005$ and $R_e/f_r = 0.2$.

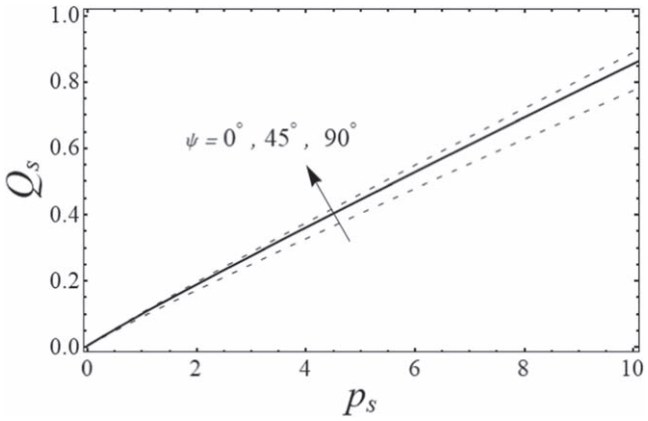

Figure 13. Change in the rate of flow with p_s as pressure gradient for distinct values of inclination angle ψ with catheter radius ratio $k = 0.5$, $n = 0.95$, $\theta = 0.1$, $U_0 = 0.005$ and $R_e/f_r = 0.2$.

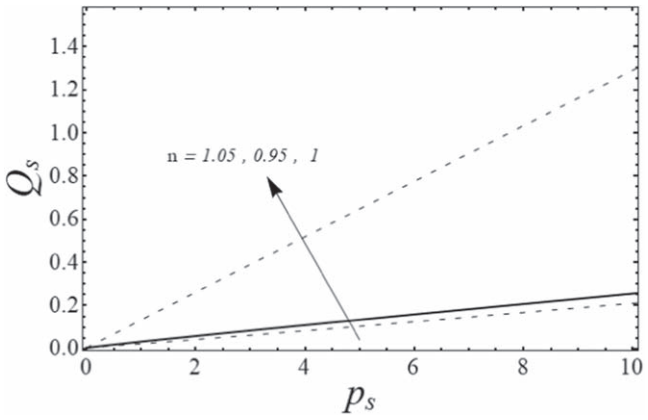

Figure 11. Change the rate of flow with p_s as pressure gradient for distinct values of n with catheter radius ratio $k = 0.5$, $\theta = 0.3$, $\psi = 45^{\circ}$, $U_0 = 0.005$ and $R_e/f_r = 0.2$.

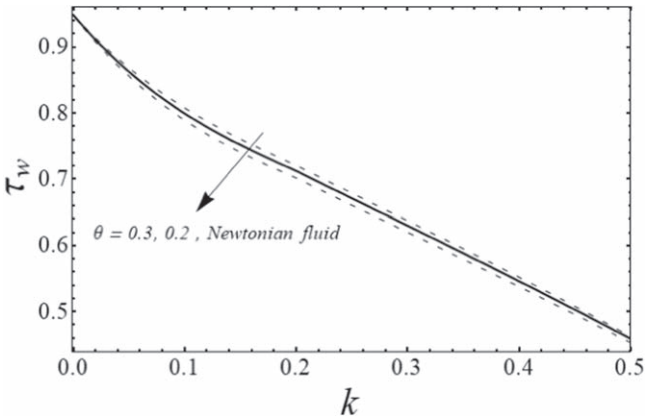

Figure 14. Change the wall shear stress with k as catheter radius ratio for distinct values of θ as yield stress with $p_s = 1$, $n = 0.95$, $\psi = 45^{\circ}$, $U_0 = 0.005$ and $R_e/f_r = 0.2$.

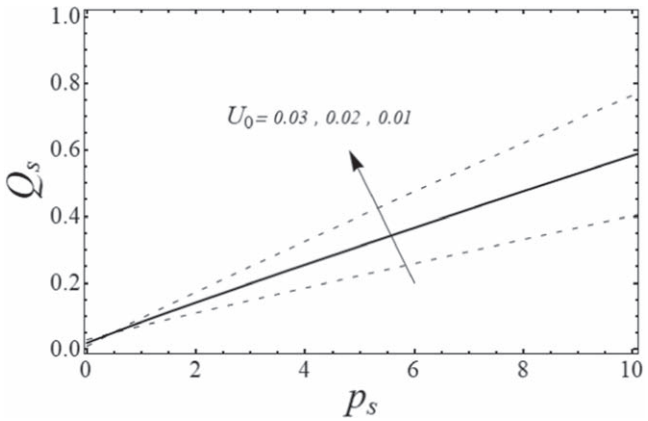

Figure 12. Change the rate of flow with p_s as pressure gradient for distinct values of slip parameter U_0 with catheter radius ratio $k = 0.5$, $n = 0.95$, $\theta = 0.1$, $\psi = 45^{\circ}$ and $R_e/f_r = 0.2$.

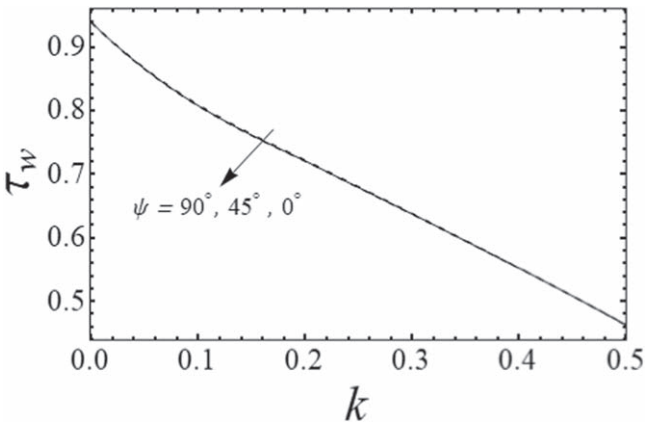

Figure 15. Change the wall shear stress with k as catheter radius ratio for distinct values of inclination angle ψ with $p_s = 1$, $n = 0.95$, $\theta = 0.3$, $U_0 = 0.005$ and $R_e/f_r = 0.2$.

a fixed catheter radius as the yield stress θ increases. Figure 15 shows the wall shear stress variations with catheter radius ratio k for distinct values of inclination angle ψ. It is observed that for the increasing values of inclination angle ψ, there is negligible increment in the wall shear stress for a specified value of catheter radius ratio k. Figure 16 shows the change in the wall shear stress with respect to catheter radius ratio k for distinct values of slip parameter U_0. It is observed that the wall shear stress grows and decreases by increasing the slip parameter U_0.

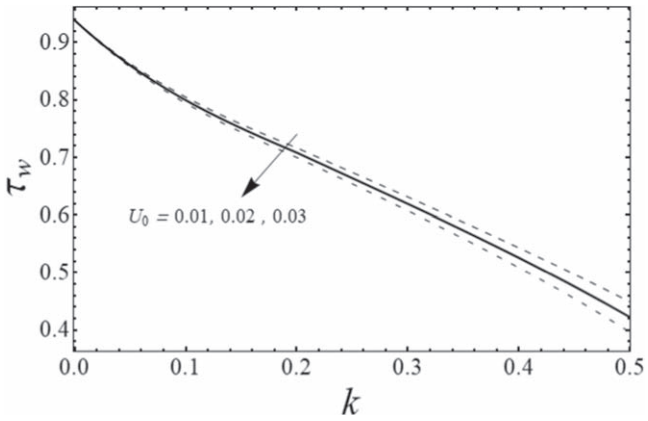

Figure 16. Change the wall shear stress with k as catheter radius ratio for distinct values of slip parameter U_0 with $p_s = 1$, $n = 0.95$, $\theta = 0.3$, $\psi = 45°$ and $R_e/f_r = 0.2$.

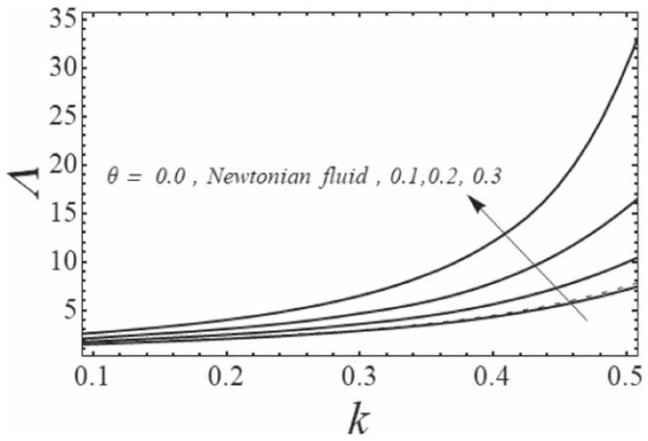

Figure 17. Change in the resistance due to friction with k as catheter radius ratio for distinct values of θ as yield stress with $p_s = 1$, $n = 0.95$, $\psi = 45°$, $U_0 = 0.005$ and $R_e/f_r = 0.2$.

Figure 17 shows the profiles of resistance to the flow with respect to catheter radius for various values of yield stress θ by fixing $n = 0.95$. The resistance to the flow for Herschel–Bulkley is greater as compared to the Newtonian and power law fluid. Also the frictional resistance for Newtonian fluid is negligibly higher than that of power law fluid.

Figure 18 shows the change in resistance to the flow with respect to catheter radius ratio k for distinct values of yield stress θ by fixing $n = 1.05$. The resistance to the flow for Herschel–Bulkley is greater as compared to the Newtonian and power law fluid. Also the resistance to the flow for Newtonian fluid is negligibly lower than that of power law fluid. Figure 19 shows the plots of resistance to the flow with respect to catheter radius k for chosen values of inclination angle ψ. It is noticed that the resistance to the flow decreases by increasing the inclination angle ψ. The effects are more prominent for higher values of k.

Figure 20 shows the change in resistance to the flow with respect to catheter radius for distinct values of slip parameter U_0. It is noticed that the resistance to the flow increased by

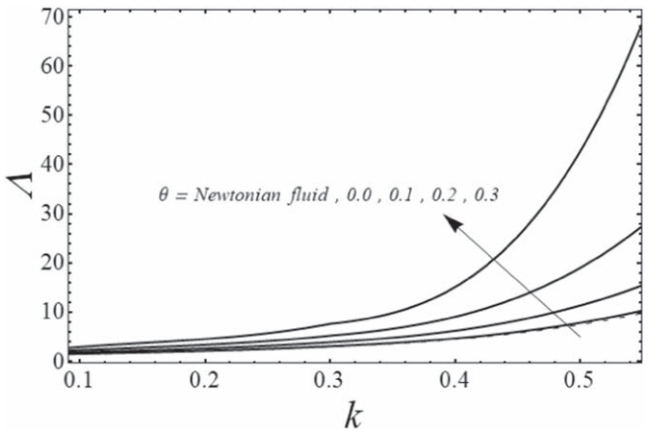

Figure 18. Change in the resistance due to friction with k as catheter radius ratio for distinct values of θ as yield stress with $p_s = 1$, $n = 1.05$, $\psi = 45°$, $U_0 = 0.005$ and $R_e/f_r = 0.2$.

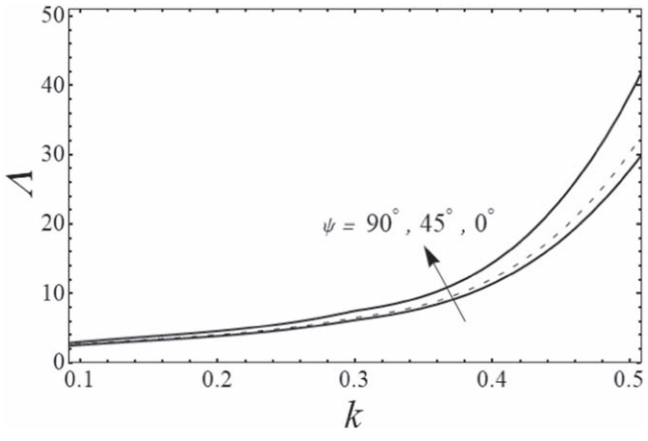

Figure 19. Change in the resistance due to friction with k as catheter radius ratio for distinct values of inclination angle ψ with $p_s = 1$, $n = 1.05$, $\theta = 0.3$, $U_0 = 0.005$ and $R_e/f_r = 0.2$.

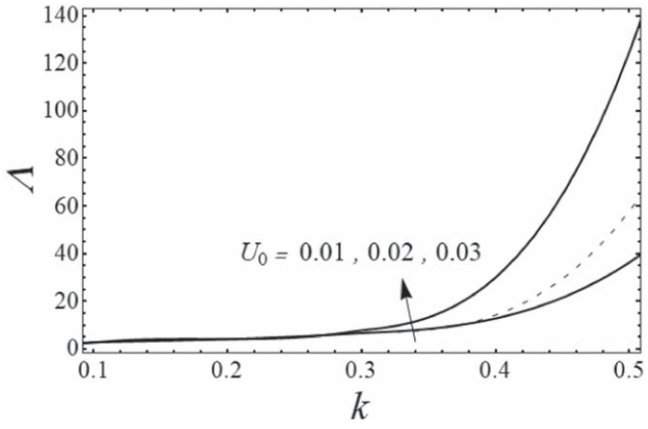

Figure 20. Change in the resistance due to friction with k as catheter radius ratio for distinct values of slip parameter U_0 with $p_s = 1$, $n = 1.05$, $\theta = 0.3$, $\psi = 45°$ and $R_e/f_r = 0.2$.

increasing the slip parameter U_0. The effects are more prominent for higher values of k.

The data for velocity change with slip parameter U_0 for $n = 0.95$ and $n = 1.05$ and the change between these values

Table 1. Variation of velocity with slip parameter U_0 with $r = 0.65$, $k = 0.5$, $\psi = 45°$, $p_s = 1$, $\theta = 0.1$, $R_e/f_r = 0.2$, when $n = 0.95$ and $n = 1.05$.

U_0	$n = 0.95$	$n = 1.05$	Difference
0.000	0.046 2163	0.040 5909	0.0562 54
0.005	0.053 4642	0.047 9657	0.0549 85
0.01	0.060 7035	0.055 3404	0.0536 31
0.02	0.075 1582	0.070 0883	0.0506 99
0.03	0.089 5844	0.084 8328	0.0475 16
0.05	0.118 36	0.114 305	0.0040 55

Table 2. Variation of velocity with inclination angle ψ with $r = 0.65$, $k = 0.5$, $U_0 = 0.005$, $p_s = 1$, $\theta = 0.1$, $R_e/f_r = 0.2$, when $n = 0.75$ and $n = 0.95$.

ψ	$n = 0.75$	$n = 0.95$	Difference
0°	0.064 3604	0.047 2225	0.017 1379
15°	0.065 7925	0.050 9556	0.014 8369
30°	0.067 1179	0.052 3059	0.013 8120
45°	0.068 2491	0.053 4642	0.014 7849
60°	0.069 1133	0.054 3521	0.014 7612

are presented in table 1. We observed that there is not considerably of difference in the variation of velocities when $U_0 = 0.05$ for $n = 0.95$ and $n = 1.05$, hence a parallel pattern is observed. So typical values of power index n are taken when $n < 1$ as 0.95 and 1.05 when $n > 1$. The data for distinction of velocity with inclination angle ψ for $n = 0.95$ and $n = 1.05$ and the change between these values are presented in table 2. It is noticed that the flow velocity for $n = 0.75$ and $n = 0.95$ increases for increasing inclination angle ψ but the variation in the difference of the velocities is very small.

5. Conclusions

In this paper the influence of non-Newtonian nature of blood and catheterization on the steady flow of blood through a uniform a inclined artery has been studied. The variation of velocity, wall shear stress, resistance of flow with respect to involved parameters is analyzed mathematically and is expressed in terms of graphs. The following conclusions have been obtained based on the graphical and tabular results.

- When the yield stress is increased, the plug core area width is increased and the velocity is decreased.
- The Herschel–Bulkley experiences lower velocity as compared to that of power law fluid.
- The flow rate shows direct relation with the pressure gradient p_s while the inverse relationship of flow rate is observed with the catheter radius ratio k and yield stress θ. Also slip velocity parameter U_0 and the inclination parameter ψ enhance the flow rate.
- Wall shear stress shows direct relationship with the yield stress θ but the situation reversed for slip parameter U_0.
- The resistance to the flow for a specific value of p_s and n increases with growing yield stress θ as well as growing catheter radius as anticipated. Also it shows decreasing trend for higher values of inclination parameter ψ.
- The values of resistance to the flow for Herschel–Bulkley fluid are greater than those of power law fluid and least for Bingham fluid.

Acknowledgments

The first and fourth authors extend their appreciation to the Deanship of Scientific Research at King Khalid University, for funding this work through research groups program under grant number R.G.P. 2/66/40.

References

[1] Daripa P and Dash R K 2002 A numerical study of pulsatile blood flow in an eccentric catheterised artery using a fast algorithms *J. Eng. Math.* **42** 1–22
[2] Back L H 1994 Estimate mean flow resistance increase during coronary artery Catheterization *J. Biomech.* **27** 169–75
[3] Toriia R, Wood N B, Hughes A D, Thom S A, Aguado-Sierra J, Davies J E, Francis D P, Parker K H and Xu X Y 2007 *J. Biomech.* **40** 2501
[4] Back L H and Denton T A 1992 Some arterial wall shear stress estimates in coronary angioplasty *Adv Bioeng.* **22** 337–40
[5] Back L H, Kwack E Y and Back M R 1996 Flow rate-pressure drop relation in coronary angioplasty: catheter obstruction effect *J. Biomech. Eng. Trans. ASME* **118** 83–9
[6] Aroesty J and Gross J F 1972 Pulsatile flow in small vessels: I. Casson theory *Biorheology* **9** 33–42
[7] Chaturani P and Ponnalagar Samy R 1986 Pulsatile flow of a Casson fluid through stenosed arteries with application to blood flow *Biorheology* **23** 499–511
[8] Jayaraman G and Tiwari K 1995 Flow in a catheterized curved artery *Med. Biol. Eng. Comput.* **33** 1–6
[9] Karahalios G T 1990 Some possible effects of a catheter on the arterial wall *Med. Phys.* **17** 922–5
[10] Dash R K, Jayaraman G and Metha K N 1996 Estimation of increased flow resistance in a narrow-catheterized artery—a theoretical model *J. Biomech.* **29** 917–30
[11] Dash R K, Jayaraman G and Metha K N 1999 Flow in a catheterized curved artery with stenosis *J. Biomech.* **32** 49–61
[12] Daripa P and Dash R K 2002 A numerical study of pulsatile blood flow in an eccentric catheterized artery using a fast algorithm *J. Eng. Math.* **42** 1–22
[13] Vajravelu K, Sreenadh S and Ramesh Babu V 2005 Peristaltic transport of a Herschel–Bulkley fluid in an inclined tube *Int. J. Nonlinear Mech.* **40** 83–90
[14] Sankar D S and Hemalatha K 2007 Pulsatile flow of Herschel-Bulkley fluid through catheterized arteries- a mathematical model *Appl. Math. Model.* **31** 1497–517
[15] Scott Blair G W and Spanner D C 1974 *An Introduction to Biorheology* (Amsterdam: Elsevier Scientific Publishing Company)
[16] Tu C and Deville M 1996 Pulsatile flow of non-Newtonian fluids through arterial stenosis *J. Biomech.* **29** 7
[17] Scott Blair G W 1966 The success of Casson equation *Rheol. Acta* **5** 184–7
[18] Iida N 1978 Influence of plasma layer on steady blood flow in microvessels *Japan. J. Appl. Phys.* **17** 203–14

[19] Zaman A, Ali N and Anwar Beg O 2016 Numerical simulation of unsteady micropolar hemo-dynamics in a tapered catheterized artery with a combination of stenosis and aneurysm *Med. Biol. Eng. Comput.* **54** 1423–36
[20] Abbas Z, Shabbir M S and Ali N 2017 Analysis of rheological properties of Herschel–Bulkley fluid for pulsating flow of blood in ω-shaped stenosed artery *AIP Adv.* **7** 105123
[21] Shabbir M S, Ali N and Abbas Z 2018 Unsteady blood flow of non-Newtonian fluid through a rigid artery in the presence of multi-irregular stenosis *J. Braz. Soc. Mech. Sci. Eng.* **40** 413
[22] Chitra M and Karthikeyan D 2018 Mathematical modeling of power law and Herschel – Bulkley non-Newtonian fluid of blood flow through a stenosed artery with permeable wall: effects of slip velocity *J Phys.: Conf. Ser.* **1000** 012064
[23] Prasad k K M and Radhakrishnamacharya G 2008 Flow of Herschel{Bulkley uid through an inclined tube of non-uniform cross-section with multiple stenosis *Arch. Mech.* **60** 161–72
[24] Ramzan M, Bilal M, Chung J D and Mann A B 2018 On MHD radiative Jefffery nanofluid flow with convective heat and mass boundary conditions *Neural Comput. Appl.* **30** 2739
[25] Ramzan M, Bilal M, Farooq U and Chung J D 2016 Mixed convective radiative flow of second grade nanofluid with convective boundary conditions: An optimal solution *Results Phys.* **6** 796–804
[26] Ramzan M, Inam S and Shehzad S A 2016 Three dimensional boundary layer flow of a viscoelastic nanofluid with Soret and Dufour effects *Alexandria Eng. J.* **55** 311–9
[27] Ramzan M and Bilal M 2016 Three-dimensional flow of an elastico-viscous nanofluid with chemical reaction and magnetic field effects *J. Mol. Liq.* **215** 212–20
[28] Tripathi B and Sharma B K 2018 Effect of variable viscosity on MHD inclined arterial blood flow with chemical reaction *Int. J. Appl. Mech. Eng.* **23** 767–85
[29] Srivastava N 2018 Herschel–Bulkley magnetized blood flow model for an inclined tapered artery for an accelerated body *J. Sci. Technol.* **10** 53–9
[30] Sankar D S and Hemalatha K 2007 A non-Newtonian fluid flow model for Blood flow through a catheterized artery–steady flow *Appl. Math. Model.* **31** 1847–64
[31] Kapura J N 1992 Mathematical model in biology and medicine (New Delhi India: East–West Press Pvt Ltd) pp 368–9